Research Article | Vol. 7, No. 10 | 1 Oct 2017 | OPTICAL MATERIALS EXPRESS 3608
Optical Materials EXPRESS

Lithography-free thin-titanium-nanocone metamaterial perfect absorbers using ZnO nanostructures

ALBERT LIN,[1,2] PARAG PARASHAR,[1,3] CHIH-CHIEH YANG,[1] DING RUNG JIAN,[1] WEI-MING HUANG,[1] YI-WEN HUANG,[1] AND TSEUNG-YUEN TSENG[1,4]

[1]*Department of Electronic Engineering, National Chiao-Tung University, Hsinchu 30010, China*
[2]*hdtd5746@gmail.com*
[3]*paragparashar03@gmail.com*
[4]*tseng@cc.nctu.edu.tw*

Abstract: In this work, thin Ti nanocones are deposited on top of the arrays of ZnO nanopagodas, and the whole structure works as an efficient nanostructured metamaterial perfect absorber (MPA) without using lithography and dry etching. In this design, ~1μm long ZnO nanopagoda arrays are grown on a 100 nm ZnO buffer layer over the silicon/glass substrate by a treatment with an aqueous solution of L-ascorbic acid. Growth direction and the degree of lamination in the ZnO nanostructures can be easily controlled by adjusting the concentration of L-ascorbic acid. Afterward, these ZnO nanopagodas are coated with a 30nm thin top and a 500nm thick bottom layer of Ti to achieve the proposed nanocone resonant cavity structure with electromagnetic wave field penetration. The overall structure encapsulates three physical concepts, namely, field penetration, adiabatic coupling and cavity resonance, which contribute the broadband perfect absorption. The entire process is carried out at a low temperature (<90°). We believe the proposed tapered Ti nanocones MPA structure facilitates ultra-broadband perfect spectral absorption with promising nature of low-cost, large-area, and lithography-free.

OCIS codes: (160.4236) Nanomaterials; (130.3990) Micro-optical devices; (160.3918) Metamaterials; (310.6845) Thin film devices and applications.

References and links

1. C. Wu, B. Neuner III, J. John, A. Milder, B. Zollars, S. Savoy, and G. Shvets, "Metamaterial-based integrated plasmonic absorber/emitter for solar thermo-photovoltaic systems," J. Opt. **14**(2), 024005 (2012).
2. X. Liu, T. Tyler, T. Starr, A. F. Starr, N. M. Jokerst, and W. J. Padilla, "Taming the blackbody with infrared metamaterials as selective thermal emitters," Phys. Rev. Lett. **107**(4), 045901 (2011).
3. N. Liu, M. Mesch, T. Weiss, M. Hentschel, and H. Giessen, "Infrared perfect absorber and its application as plasmonic sensor," Nano Lett. **10**(7), 2342–2348 (2010).
4. D. Dregely, R. Taubert, J. Dorfmüller, R. Vogelgesang, K. Kern, and H. Giessen, "3D optical Yagi-Uda nanoantenna array," Nat. Commun. **2**, 267 (2011).
5. C. M. Watts, X. Liu, and W. J. Padilla, "Metamaterial electromagnetic wave absorbers," Adv. Mater. **24**(23), OP98–OP120, OP181 (2012).
6. W. H. Emerson, "Electromagnetic wave absorbers and anechoic chambers through the years," IEEE Trans. Antenn. Propag. **21**(4), 484–490 (1973).
7. C. Argyropoulos, K. Q. Le, N. Mattiucci, G. D'Aguanno, and A. Alu, "Broadband absorbers and selective emitters based on plasmonic Brewster metasurfaces," Phys. Rev. B **87**(20), 205112 (2013).
8. J. Zhou, A. F. Kaplan, L. Chen, and L. J. Guo, "Experiment and theory of the broadband absorption by a tapered hyperbolic metamaterial array," ACS Photonics **1**(7), 618–624 (2014).
9. K. X. Wang, Z. Yu, V. Liu, M. L. Brongersma, T. F. Jaramillo, and S. Fan, "Nearly total Solar absorption in ultrathin nanostructured iron oxide for efficient photoelectrochemical water splitting," ACS Photonics **1**(3), 235–240 (2014).
10. D. Ji, H. Song, X. Zeng, H. Hu, K. Liu, N. Zhang, and Q. Gan, "Broadband absorption engineering of hyperbolic metafilm patterns," Sci. Rep. **4**(1), 4498 (2015).
11. K. Aydin, V. E. Ferry, R. M. Briggs, and H. A. Atwater, "Broadband polarization-independent resonant light absorption using ultrathin plasmonic super absorbers," Nat. Commun. **2**, 517 (2011).
12. H. Tao, C. M. Bingham, D. Pilon, K. Fan, A. C. Strikwerda, D. Shrekenhamer, W. J. Padilla, X. Zhang, and R. D. Averitt, "A dual band terahertz metamaterial absorber," J. Phys. D Appl. Phys. **43**(22), 225102 (2010).

#301712 https://doi.org/10.1364/OME.7.003608
Journal © 2017 Received 10 Jul 2017; revised 3 Sep 2017; accepted 13 Sep 2017; published 18 Sep 2017

Optical Materials EXPRESS

13. Q.-Y. Wen, H.-W. Zhang, Y.-S. Xie, Q.-H. Yang, and Y.-L. Liu, "Dual band terahertz metamaterial absorber: Design, fabrication, and characterization," Appl. Phys. Lett. **95**(24), 241111 (2009).
14. Y. K. Zhong, S. M. Fu, N. P. Ju, M. Tu, B. Chen, and A. Lin, "Fully planarized perfect metamaterial absorbers with no photonic nanostructures," IEEE Photonics J. **8**(1), 2200109 (2016).
15. Y. Cui, K. H. Fung, J. Xu, H. Ma, Y. Jin, S. He, and N. X. Fang, "Ultrabroadband light absorption by a sawtooth anisotropic metamaterial slab," Nano Lett. **12**(3), 1443–1447 (2012).
16. Y.-K. R. Wu, A. E. Hollowell, C. Zhang, and L. J. Guo, "Angle-insensitive structural colours based on metallic nanocavities and coloured pixels beyond the diffraction limit," Sci. Rep. **3**(1), 1194 (2013).
17. G. Subramania, S. Foteinopoulou, and I. Brener, "Nonresonant broadband funneling of light via ultrasubwavelength channels," Phys. Rev. Lett. **107**(16), 163902 (2011).
18. C. Zhang, H. Subbaraman, Q. Li, Z. Pan, J. G. Ok, T. Ling, C.-J. Chung, X. Zhang, X. Lin, R. T. Chen, and L. J. Guo, "Printed photonic elements: nanoimprinting and beyond," J. Mater. Chem. C Mater. Opt. Electron. Devices **4**(23), 5133–5153 (2016).
19. L. Gao, K. Shigeta, A. Vazquez-Guardado, C. J. Progler, G. R. Bogart, J. A. Rogers, and D. Chanda, "Nanoimprinting techniques for large-area three-dimensional negative index metamaterials with operation in the visible and telecom bands," ACS Nano **8**(6), 5535–5542 (2014).
20. W.-C. Y. Y.-C. Chang, C.-M. Chang, P.-C. Hsu, and L.-J. Chen, "Controlled Growth of ZnO Nanopagoda Arrays with Varied Lamination and Apex Angles," Cryst. Growth Des. **9**(7), 3161–3167 (2009).
21. Y. Liu, G. Liu, Y. Wang, W. Gao, H. Hao, and B. Huang, "Multistep Controllability Synthesis and Growth Mechanism of ZnO Nanopagoda for Schottky Diode Device," Nano **11**(02), 1650024 (2016).
22. Y.-C. Chang, "Temperature-dependence cathodoluminescence of ultra-sharp ZnO nanopagoda arrays," J. Alloys Compd. **617**, 16–20 (2014).
23. H.-M. Chiu and J.-M. Wu, "Opto-electrical properties and chemisorption reactivity of Ga-doped ZnO nanopagodas," J. Mater. Chem. A Mater. Energy Sustain. **1**(18), 5524 (2013).
24. D. Panda and T.-Y. Tseng, "One-dimensional ZnO nanostructures: fabrication, optoelectronic properties, and device applications," J. Mater. Sci. **48**(20), 6849–6877 (2013).
25. G. Wang, Z. Ye, H. He, H. Tang, and J. Li, "Growth and properties of ZnO/hexagonal ZnMgO/cubic ZnMgO nanopagoda heterostructures," J. Phys. D Appl. Phys. **40**(17), 5287–5290 (2007).
26. Rsoft, *Rsoft CAD User Manual,* 8.2 ed. (Rsoft Design Group, 2010).
27. Y. K. Zhong, Y.-C. Lai, M.-H. Tu, B.-R. Chen, S. M. Fu, P. Yu, and A. Lin, "Omnidirectional, polarization-independent, ultra-broadband metamaterial perfect absorber using field-penetration and reflected-wave-cancellation," Opt. Express **24**(10), A832–A845 (2016).

1. Introduction

Metamaterial perfect absorbers (MPAs) are devices that are designed to absorb incident electromagnetic radiations efficiently. The nascent field of metamaterial perfect absorbers (MPAs) is studied comprehensively in recent years due to their numerous applications in diverse technological fields such as thermophotovoltaics [1], thin-film thermal emitters [2], sensors and detectors [3], antenna systems [4] and biomedical optics [5,6]. Significant advancements directed for broadband absorption MPAs has been achieved in the past [7–14]. In most of these works, implementation of metals as the absorbing materials has been a vital component due to their high extinction coefficients over a wide spectral regime. However, large refractive index dissimilarity between metal and the surroundings led to the coupling mismatch for the incoming electromagnetic radiations. Thus, there have been many attempts to eradicate this disparity, and this, in turn, leads to the originations of different schemes in order to enhance photon confinement and photon coupling at various metallic structures to achieve perfect broadband absorption. Various noted schemes in this regard include the condensed field intensity using localized surface plasmon polariton (SPP) by Atwater et al. [11], the adiabatically-coupled tapered hyperbolic metamaterial (HMM) ultra-broadband absorber by Fang et al. [15], simulation-based plasmonic Brewster metasurface metallic nanocones [7], photonics funneling effect [16,17], and an omnidirectional, polarization-independent ultra-broadband MPA structure based on field penetration [14].

Although all of these schemes provided some advances in enhancing absorption over broad spectral regimes via coupling matching, there have been a few limitations as well. Electron beam lithography based plasmonic perfect absorbers [11] suffered from wavelength scalability issues along with some difficulty in achieving ultra-broad bandwidth due to the evident material dispersion phenomenon. Similarly, enhanced omnidirectionality with broad spectral range had been achieved by adiabatically-coupled tapered hyperbolic metamaterial

Optical Materials EXPRESS

(HMM) ultra-broadband absorbers [15], yet, low scalability to large-area fabrication and repetitive use of focused ion beam (FIB) lithography [10] and etching techniques were present in this tapered HMM design. Slow e-beam and FIB lithography used in these works lead to cost and time inefficiency towards the realization of low-cost, large-area and complexity-free designs. On the other hand, field penetration based flat MPA structure [14] does not require lithography and etching techniques, but unlike the tapered HMM MPA [15], the absorption values achieved is only nearly-prefect in this work and requires repeated metal-dielectric stacking. A nano-imprint based tapered HMM MPA by J.Guo et al. [8] eliminates the use of multiple lithography steps for the tapered hyperbolic metamaterial (HMM) ultra-broadband absorbers [15], and the method is suitable for large area fabrication [18,19]. While significant advancements have been achieved in the past, ultimate aims remained to attain lithography and dry etching free, low-cost, low-temperature, and low-complexity designs with ultra-broadband absorption.

In recent years, ZnO has been widely recognized as a versatile material with numerous applications in electronics and optoelectronics technological fields [20]. Typically, ZnO films are formed via various fabricating methods including pulsed laser deposition, thermal evaporation, spray pyrolysis, metal organic chemical vapor deposition, radio frequency magnetron sputtering, and epitaxial electrodeposition. Nonetheless, an alternating aqueous chemical growth (ACG) based fabrication technique has been found to be an efficient method to grow low-cost three-dimensional (3D) ZnO nanotubes, ZnO nanorods, ZnO nanowires, ZnO nanoplates, ferric oxide nanorods, tin dioxide nanorods, and arrays of ZnO nanopagoda [21–25].

In the proposed work here, thin-metal on ZnO nanopagoda MPA structure has been investigated. ZnO nanopagoda arrays grown on the silicon substrate by adding L-ascorbic acid have been used as a base to incorporate gradient index thin Ti nanocones, as shown in Fig. 1. This gradient profile structure will facilitate proper adiabatic coupling of the incoming photons into the structure. Our tapered structure does not require cost and time-consuming lithography and dry plasma etching techniques as compared to the tapered HMM structures [15]. Besides, this design does not suffer from wavelength scalability and material dispersion issues as compared to plasmonic-based perfect absorbers [11]. Due to the nanostructure, light scattering and diffraction enhance the broadband absorption while these are impossible in a planar structure [14]. Figure 2 illustrate the various concepts of physics involved in our structure.

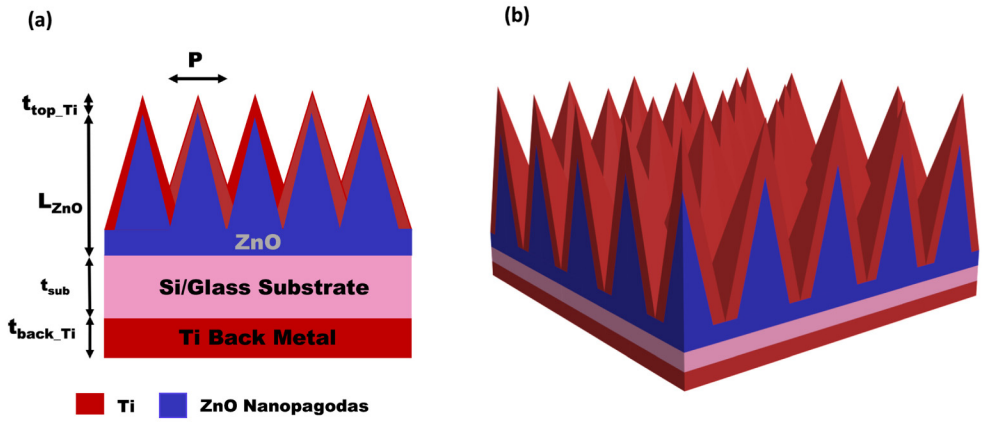

Fig. 1. (a) Two-dimensional (2D) and (b) three-dimensional (3D) cross-sectional views of our proposed MPA structure.

Optical Materials EXPRESS

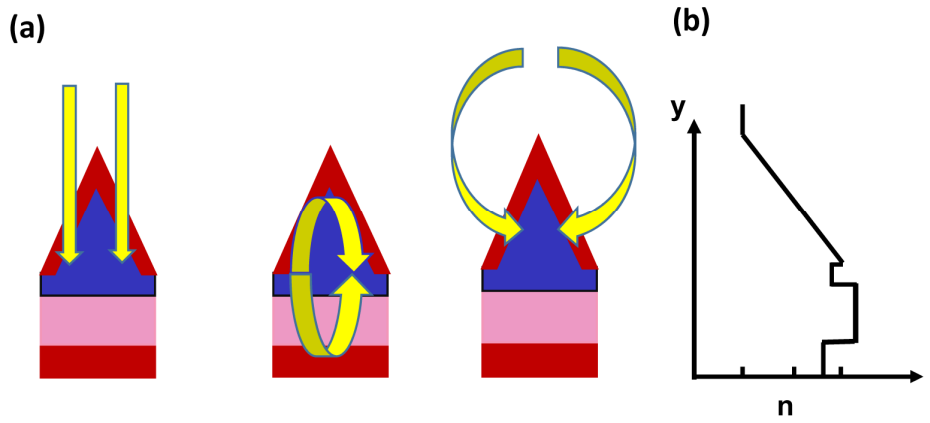

Fig. 2. (a) Physical concepts involving field penetration, resonant cavity, and adiabatic coupling for the proposed design. (b) The gradient index variation is also shown along the vertical y direction. n is the refractive index, and y is the vertical space coordinate. The gradient index is the key to adiabatic coupling.

2. Methods

2.1 Theoretical modeling and optimization

Rigorous coupled wave analysis (RCWA) method in Rsoft Diffractmod™ has been adopted for simulations in this work. Material parameters from the Rsoft database have been used here [26]. RCWA is a numerical method in computational electromagnetics, which implements eigenmode expansion where the waveguide modes in the layered structure are the bases for the solution fields in the periodic nanostructures.

2.2 Sample fabrication

In the first phase, a t_{sub} = 675μm thick Si or a glass substrate is cleaned ultrasonically in isopropyl alcohol (IPA), acetone and distilled water for 10 minutes, separately. After that, t_{buffer} = 100nm thin epitaxial ZnO buffer layer was deposited by KD RF sputtering method at room temperature. RF sputtering has been operated at 3×10^{-6} torr pressure. The basic ZnO nanorod arrays were then grown downwards by immersing pre-modified substrates into the precursor solution for 1 hour at 90°C. 0.025 M methenamine ($C_6H_{12}N_4$, 99.9% purity) and 0.025 M zinc nitrate hexahydrate ($Zn(NO_3)_26H_2O$, 99.9% purity) were mixed in proportions for the preparation of precursor solution. As the temperature of the solution is increased, $C_6H_{12}N_4$ begins to dissolve into water and produce ammonia. Afterward, ammonia starts to be dissolved into water.

$$(CH_2)_6N_4 + 6H_2O \rightarrow 6HCHO + 4NH_3 \quad (1)$$

$$NH_3 + H_2O \rightarrow NH_4^+ + OH^- \quad (2)$$

Eventually, hydroxyl ions start a chemical reaction with Zn^{2+}, and $Zn(OH)_4^{2-}$ is formed. Then, ZnO nuclei start accumulating slowly on the substrate, and the ZnO nanorods begin to grow vertically.

$$4OH^- + Zn^{2+} \rightarrow Zn(OH)_4^{2-} \quad (3)$$

$$Zn(OH)_4^{2-} \rightarrow ZnO_{(s)} + H_2O + 2OH^- \quad (4)$$

These ZnO nanorods were subsequently converted into pagoda morphologies by placing the substrate with the basic nanorod arrays downward near the surface of a chemical solution and heated to about 90°C for 3 hours. This chemical solution contains 2.75 × 10–4M L-

Optical Materials EXPRESS

ascorbic acid ($C_8H_8O_6$, 99% purity) along with 0.01 M zinc nitrate hexahydrate ($Zn(NO_3)_26H_2O$, 99.9% purity), and 0.01 M methenamine ($C_6H_{12}N_4$, 99.9% purity).

In the second phase, an ultra-thin t_{top_Ti} = 30 nm metal Ti layer is deposited on top of arrays of ZnO nanopagodas for the formation of nanocones via electron-gun (e-gun) evaporation. After that, the sample is rotated, and a thick t_{back_Ti} = 500nm layer is deposited at the substrate back side through e-gun evaporation for the cavity formation. Our overall proposed design is carried out at low temperature (90°C) with minimal equipment required. More importantly, entire process does not require any lithography and dry etching steps.

2.3 Sample measurements

The reflectance (R) and transmittance (T) are measured by ultraviolet visible near-infrared (UV-VIS-NIR) spectroscopy using Hitachi U-4100 with a built-in integration sphere. Absorption (A) can be calculated by the formula Absorption (A) = 1-Reflectance (R)-Transmittance (T). The detailed measurement drawing can be referred in our past publication [27]. SEM and STEM-EDS micrographs data has been collected by Hitachi SU-8010 and OXFORD INCA, respectively. A 15kV energy beam has been used for the SEM data.

3. Results and discussion

3.1 Simulation results

Thin Ti nanocones on top of ZnO nanopagodas along with the incorporated back side Ti metal layer introduce physical concepts of field penetration and the resonant cavity into the structure, as shown in Fig. 2. A reduced glass substrate thickness t_{sub} = 1µm is used instead of a thick substrate layer in Fig. 3 and Fig. 4 in order to plot the entire structure field profiles. On the other hand, in Fig. 5 simulation data, the glass/Si substrates of t_{sub} = 675µm is used in the calculation to compare the simulation and experiment results. The tapered metal nanocones along with the ZnO nanopagoda arrays facilitate gradient index structure, and this leads to the adiabatic coupling phenomenon into the device. A relatively thick t_{back_Ti} = 500nm layer at the back side is responsible for the cavity formation as well as for the back reflectance in order to eliminate transmittance. Absorption spectrum curves for the simulated structure have been shown in Fig. 3. Various combinations of Ti thickness (t_{top_Ti}) and ZnO nanopagoda lengths (L_{ZnO}) have been employed in the simulations. It can be seen that high absorption (>0.95) is maintained in the ultraviolet visible near-infrared (UV-VIS-NIR) regime especially for ZnO length L_{ZnO} = 5µm where a close-to-perfection absorption curve is attained up to λ = 2µm for t_{top_Ti} = 100 nm and L_{ZnO} = 5µm. The origin of oscillations in these profiles can be accredited to the presence of resonance phenomenon occurring in the resonant cavity formed by the top Ti and bottom Ti layers. Also, the oblique incidence absorption curves for the S and P polarizations are included at the right of Fig. 3. It can be seen that the absorption does not degrade significantly at 60° incidences. This indicates the Ti/ZnO nanopagoda MPA is an omnidirectional device. The p-polarized light degrades more than s-polarized light is. The phenomenon can be understood by knowing that the electric field direction changes with the incidence angle for p-polarization. Thus, the performance deviation from the normal incidence is more pronounced in the p-polarized light. On the other hand, as the incidence angle changes, the electric field direction is still in the horizontal direction for the s-polarization, i.e. parallel to the wafer surface, and thus the 60° oblique incidence absorption does not degrade much for the s-polarized light.

Figure 4 depicts the field profiles for our proposed Ti nanocone MPA structure. The origin of the absorption lies in the adiabatic coupling of the incident photons by the tapered ZnO pagodas and the cavity confinement by the top and bottom Ti layers while the photon absorption happens in the Ti layer. High electric field intensity on the nanocone slopes in Fig. 4(a) is observed, and this can be attributed to the adiabatic coupling in the structure, thereby, verifying the presence of adiabatic coupling phenomenon in the device. The same high

Optical Materials EXPRESS

electric field intensity on the tapered sides can also been seen in the top view of the structure, in Fig. 4(b). Beside adiabatic coupling, the standing wave patterns are observed in Fig. 4(a) due to the resonant cavity, which is beneficial for the confinement of the photons in the device. Finally, the existence of magnetic field through the Ti thin layer in Fig. 4(c) confirms the applicability of field penetration concept in our proposed structure, and the photons are absorbed in the Ti thin layers contributing to the high absorption over broadband.

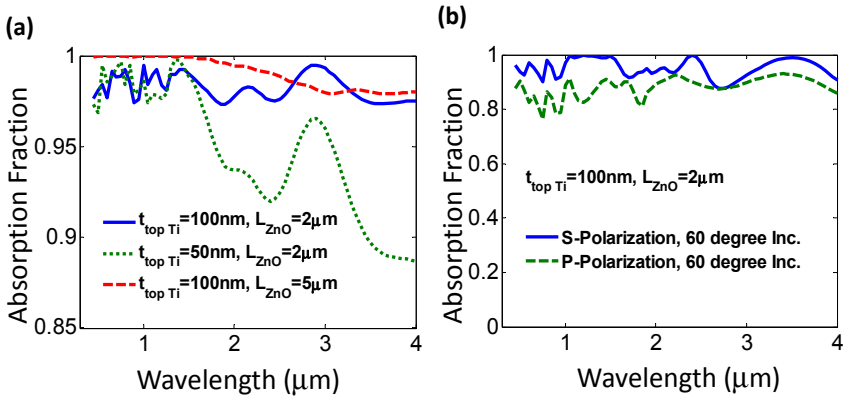

Fig. 3. The spectral absorption of the lithography-free thin-Ti nanocone MPA at (a) normal incidence and (b) 60° oblique incidence. P = 1μm. t_{back_Ti} = 500nm. A reduced glass substrate thickness t_{sub} = 1μm is used in order to plot the entire structure field profile in Fig. 4. In Fig. 5 simulation data, the glass/Si substrates of t_{sub} = 675μm is used in the calculation.

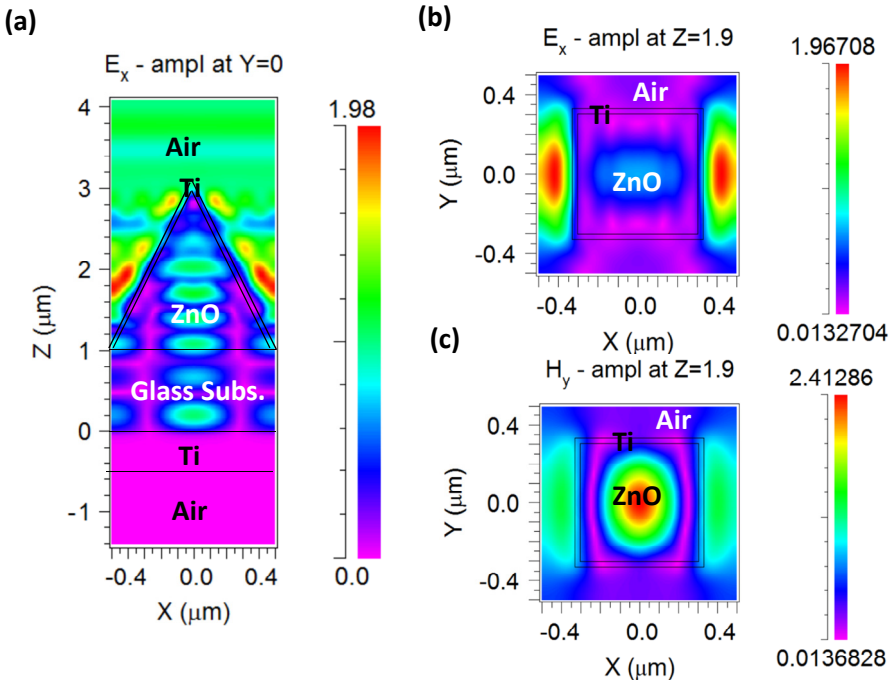

Fig. 4. The field profiles for the time harmonic steady-state electric field amplitude x-component (E_x) and magnetic field y-component (H_y) at λ = 1μm. (a) E_x at the Y = 0 plane. (b)-(c) The field profiles on X-Y plane at Z = 1.9 μm for E_x and H_y respectively. t_{top_Ti} = 100nm, L_{ZnO} = 2μm, P = 1μm, t_{back_Ti} = 500nm. A reduced glass substrate thickness t_{sub} = 1μm is used in order to plot the entire structure field profile in Fig. 4. In Fig. 5 simulation data, the glass/Si substrates of t_{sub} = 675μm is used in the calculation.

Optical Materials EXPRESS

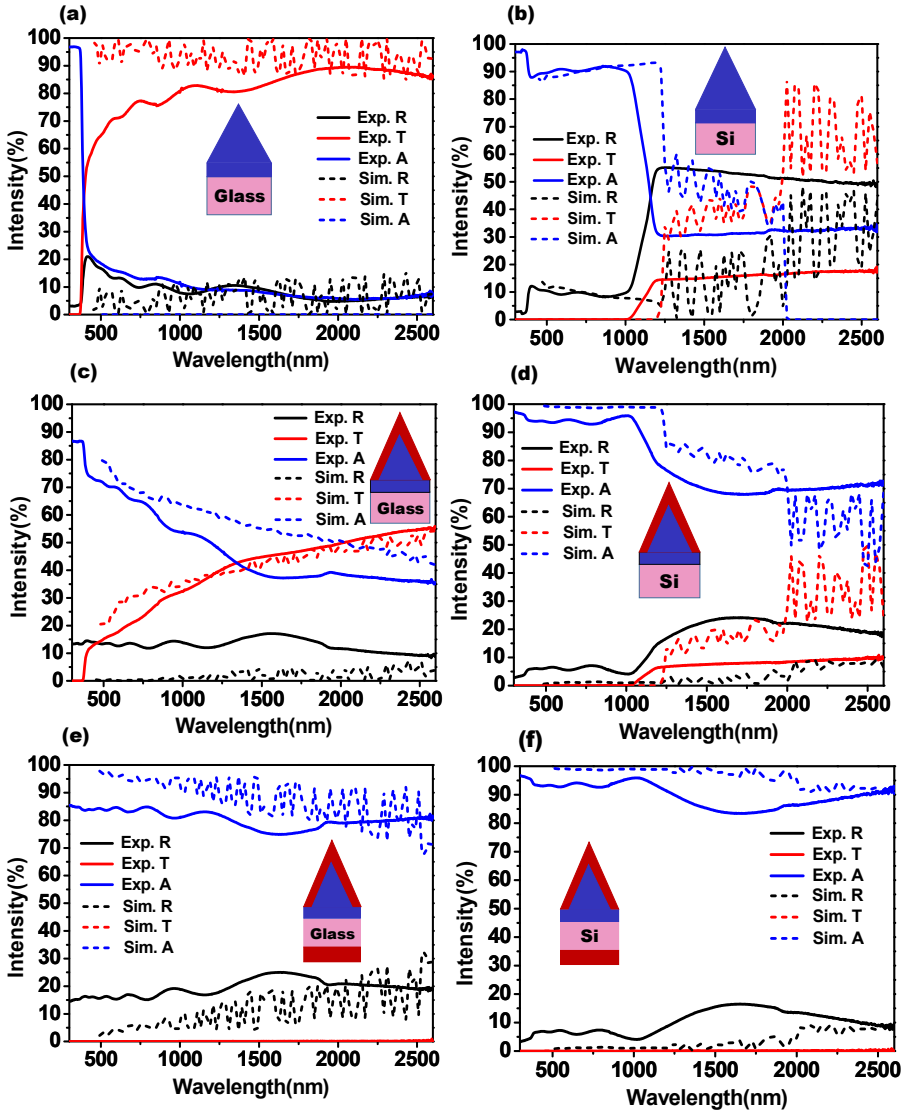

Fig. 5. Experimental (Exp.) spectral response curves for reflectance (R), transmittance (T), and absorption (A) for the proposed Ti/ZnO nanopagoda MPAs. The simulation (sim.) data is plotted in dashed line for comparison. (a) ZnO pagoda on a glass substrate (b) ZnO pagoda on a Si substrate (c) ZnO pagoda on a glass substrate with t_{top_Ti} = 30nm top Ti thin layer (d) ZnO pagoda on Si substrate with t_{top_Ti} = 30nm top Ti thin layer. (e) ZnO pagoda on glass substrate with t_{top_Ti} = 30nm top Ti thin layer and 500nm bottom Ti layer. (f) ZnO pagoda on Si substrate with t_{top_Ti} = 30nm top Ti thin layer and 500nm bottom Ti layer. For (a)-(f), t_{sub} = 675μm, L_{ZnO} ~1 μm, P = 0.3μm.

3.2 Experiment results

In this section, we present the experimental results of the proposed Ti nanocone MPA structure. Figure 5 shows the experiment results, plotting the reflectance (R), the transmittance (T) and the absorption (A) for the Ti nanocone MPA structure on the glass or Si substrates with various configurations. To achieve maximal absorption, the reflectance and the transmittance losses should be low. In Fig. 5(a), curves for the reflectance (R), the transmittance (T) and the absorption (A) have been presented for the bare ZnO nanopagoda nanostructure on a glass substrate without the top and bottom Ti metallic layers. It can be

Optical Materials EXPRESS

seen that absorption is low, and in this case, the ZnO tips act as an anti-reflectance coating (ARC) for the silicon or glass substrates. Figure 5(b) shows the ZnO pagodas on Si substrate, where the absorption below 1μm is due to the Si absorption.

Figure 5(c)-(d) represent the R, T, A curves for our proposed design with top Ti layer. Absorption has been improved as compared to Fig. 5(a)-(b) with the insertion of the top Ti thin nanocone layer as it facilitates the field penetration effect, which in turn results in Ti thin layer absorption. However, absorption value is still low in Fig. 5(c) and (d), and further improvement can be done by using the complete proposed Ti nanocone resonant cavity structure. In the absence of the resonant cavity, incomplete absorption occurs, and the transmittance can significantly reduce the absorption.

Figure 5(e)-(f) depicts the reflectance (R), the transmittance (T) and the absorption (A) for the proposed Ti nanocone MPA structure with both top and bottom Ti layer, on glass and Si substrates, respectively. High absorption (~95%) is observed in Fig. 5(f). Transmittance losses are entirely eliminated in this structure due to the incorporation of t_{back_Ti} = 500nm thick back reflector. This high absorption can be attributed to the presence of field penetration, cavity resonance, adiabatic coupling, and the gradient index variation effects in our proposed design.

The deviation of the experiment from the simulation mainly comes from that the shape of the fabricated nano-pagodas can deviate from perfect nano-cones, evident from the SEM/TEM micrographs in Fig. 6 and Fig. 7. The shape can certainly affect the performance of the design, which is reflected in the higher reflectance in the experiment than in the simulation, evident in Fig. 5(c) and 5(d). For the case of no bottom Ti reflectors in Fig. 5(b) and 5(d), there are some interference patterns from λ = 2μm to λ = 2.6μm in the simulation but not in the experiment. This is due to the wafer backside roughness makes the interference pattern less obvious in the experiment. It should be emphasized that even with the wafer backside roughness, the top and bottom Ti layers still constitute a broadband cavity for enhanced photon confinement and absorption evident from Fig. 5(f). In the case of the glass substrate, two-side polished glass substrates are used. Since the glass refractive index is not very different from air, the interference pattern is not very pronounced both in simulation and in experiment, as can be seen in Fig. 5(a) and 5(c).

The thicknesses of Ti nanocones and ZnO nanopagodas have been measured by using scanning electron microscope (SEM). SEM micrographs have been shown in Fig. 6. It can be seen from Fig. 6(a) that the ZnO nanopagoda length is around L_{ZnO} ~1 μm while the period (P) for the arrays is approximately 0.3 μm on the Si substrate. Furthermore, Fig. 6(b) shows that the ZnO nanopagodas grown on glass substrate appear flat in top and resemble nanorods instead of a nanopagodas. Therefore, the arrays of ZnO nanopagodas grown on the Si substrate is better tapered and provide better similarity to the proposed Ti nano-conical structure in this work. Without sidewall taper, the adiabatic in-coupling of the incident light is highly degraded because in this case the anti-reflection effect is solely by diffraction.

Figure 7(a)-7(b) depicts the transmittance electron microscope (TEM) data of the ZnO nanopagodas coated with Ti metal nanocones. Top Ti metal thicknesses (t_{top_Ti}) measured in Fig. 7(b) (thick red lines) are found to be around 30nm at three different places, as expected. Figure 7(c)-7(d) represents the scanning transmission electron microscope energy dispersive spectroscopy (STEM- EDS) depth and sidewall coverage data for the structure, respectively. Here, platinum (Pt) has been used as the sacrificial layer and with the help of focused ion beam technique, a thinned sample and thus site-specific analysis has been done. The atomic ratio variation with distance has been presented. In Fig. 7(c), a narrow peak of Ti around 70 nm indicates the presence of Ti nanocones on the top of the structure. Oxygen and zinc variation throughout the depth can also be seen here and points to the presence of ZnO in the proposed design. Similar curves can be observed in Fig. 7(d) for the sidewall coverage. Here, a broad peak in Ti data from 10nm to 35nm confirms the existence of Ti on the sidewall of the structure. Thus, it is observed that the experimental structure of our proposed design is

Optical Materials EXPRESS

reasonably similar to the profile adopted during simulation, validating our righteous approach towards the realization of lithography-free photonic nanostructures for MPA applications.

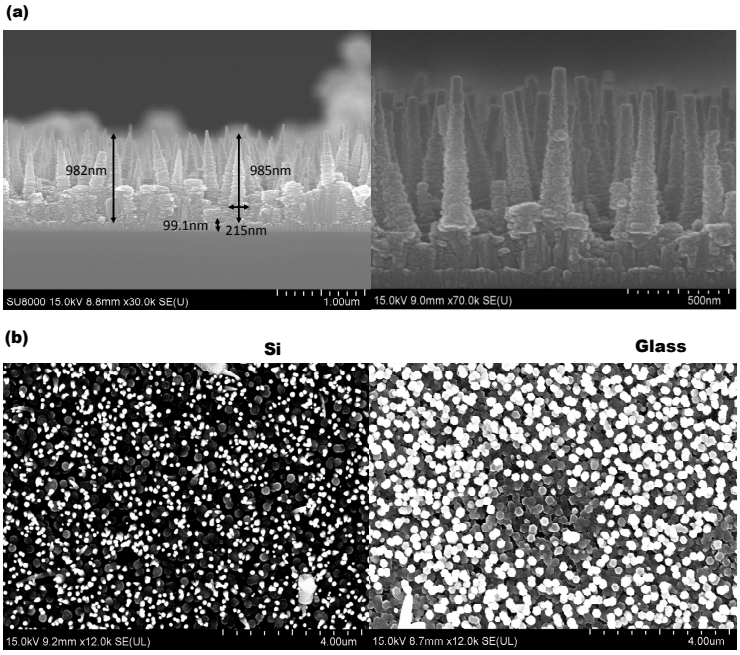

Fig. 6. (a) The scanning electron microscope (SEM) data for the side view of ZnO nanopagodas with L_{ZnO} ~1 µm length and period (P)~0.3µm on Si substrate. The zoom-in view is also shown at the right. (b) The SEM top view of the ZnO nanopagoda arrays on a Si substrate and on a glass substrate. It can be seen the flat-top nature of the ZnO pagodas on a glass substrate that hampers adiabatic light in-coupling.

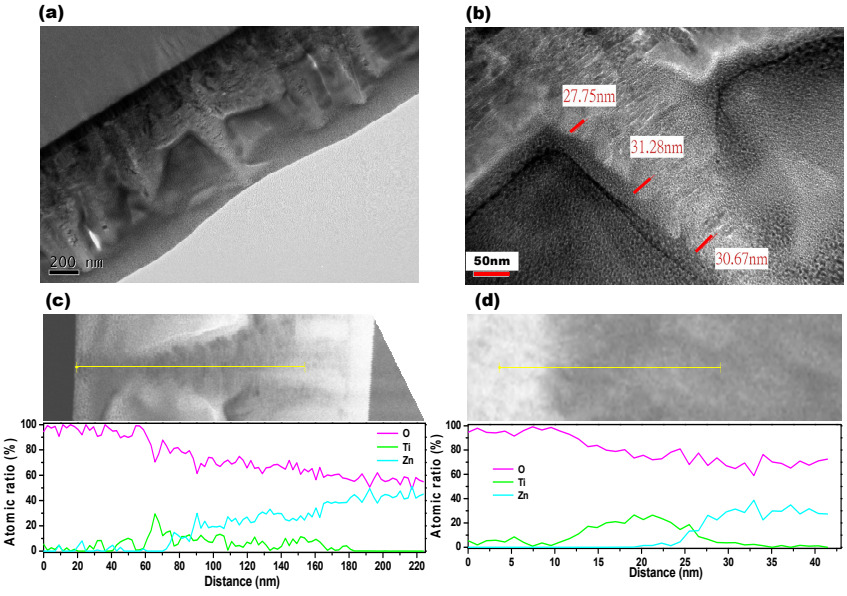

Fig. 7. (a) The transmission electron microscope (TEM) image of the ZnO nanopagodas coated with Ti metal nanocones. t_{top_Ti} = 30nm. (b) The TEM image of top Ti nanocone thickness at three places (thick red lines) (c)-(d) STEM-EDS depth and sidewall coverage data for the ZnO nanopagodas coated with Ti metal nanocones, respectively.

Optical Materials EXPRESS

4. Conclusion

A lithography-free thin-metal Ti nanocone resonant cavity metamaterial perfect absorber has been proposed in this work. Arrays of ~1μm long ZnO nanopagodas have been incorporated into the structure for the facilitation of Ti nanocones. ZnO nanopagoda arrays have been grown on the ZnO buffer layer over the silicon/glass substrates by treatment with aqueous solution of L-ascorbic acid. Thin 30 nm Ti nanocones are then deposited on these arrays of ZnO nanopagodas, and this gradient index structure works as a perfect metamaterial absorber in the ultraviolet visible near-infrared (UV-VIS-NIR) regime. High absorption is achieved throughout the UV-VIS-NIR range. Our proposed Ti nanocone MPA gradient index structure induces enhanced cavity resonance, adiabatic coupling, and field penetration effects into the structure, thereby, facilitating high absorption over a wide UV-VIS-IR regime. Besides, the low thermal budget is required by our structure as all the processes were carried at relatively low temperature (90°C). The most significant advantage of our proposed design is the elimination of lithography and etching processes, thereby, paving the way for low-cost, low-complexity and large-area industrial scale fabrication. Our future endeavors will be directed toward achieving ZnO nanopagoda length in excess of 2μm through low-temperature processes such as chemical bath deposition, hydrothermal approaches, and sol-gel.

Funding

Ministry of Science and Technology (MOST), Taiwan (MOST 104-2221-E-009 −115 -MY2).

Acknowledgments

Albert Lin and Tseung-Yuen Tseng organized the research project, performed RCWA calculation, and analyzed the experimental and simulation results. Parag Parashar and Ding-Rung Jian performed the UV-VI-NIR spectroscopy measurement. Ding-Rung Jian performed sample fabrication and SEM/STEM-EDS analysis. Parag Parashar wrote the manuscript and prepared the figure files. Albert Lin and Parag Parashar have equal contribution to this work.

Disclosures

Competing financial interests: The authors declare no competing financial interests.